MoS_2 monolayer catalyst doped with isolated Co atoms for the hydro-deoxygenation reaction

Guoliang Liu[1], Alex W. Robertson[2], Molly Meng-Jung Li[1], Winson C. H. Kuo[1], Matthew T. Darby[3], Mohamad H. Muhieddine[3], Yung-Chang Lin[4] , Kazu Suenaga[4], Michail Stamatakis[3], Jamie H. Warner[2], Shik Chi Edman Tsang[1]*

[1]Wolfson Catalysis Centre, Department of Chemistry, University of Oxford, Oxford, OX1 3QR, UK.
[2]Department of Materials, University of Oxford, Oxford OX1 3PH, UK.
[3]Thomas Young Centre and Department of Chemical Engineering, University College London, London WC1E 7JE, UK.
[4]National Institute of Advanced Industrial Science and Technology (AIST), Central 5, 1-1-1 Higashi, Tsukuba, Ibaraki 305-8565, Japan

*Correspondence to: edman.tsang@chem.ox.ac.uk.

The conversion of oxygen-rich biomass into hydrocarbon fuels requires efficient hydro-deoxygenation catalysts during the upgrading process. However, traditionally prepared Co-MoS_2 catalysts, although efficient for hydro-desulfurisation, are not appropriate due to their poor activity, sulfur loss and rapid deactivation at elevated temperature. Here, we report the synthesis of MoS_2 monolayer sheets decorated with isolated Co atoms through covalent bonding of Co to sulfur vacancies on the basal planes that, when compared to conventionally prepared samples, exhibit superior activity, selectivity and stability for the hydro-deoxygenation of 4-methylphenol to toluene. The higher activity, allows the reaction temperature to be reduced from the typically used 300 ^{o}C to 180 ^{o}C and thus allows the catalysis to proceed without sulfur loss and deactivation. Experimental analysis and density functional theory calculations reveal a large number of sites at the interface between the Co and Mo atoms on the MoS_2 basal surface and we ascribe the higher activity to the presence of sulfur vacancies that are created local to the observed Co-S-Mo interfacial sites.

Sulfided CoMo or NiMo catalysts have been commercially used for hydro-desulfurisation reactions for decades[1,2]. It is generally believed that active sites on the crystallographic edges of MoS_2 slabs, promoted by Co or Ni atoms, can activate organic sulfides and H_2 for the catalytic removal of sulfur in hydrocarbon streams[3,4]. The catalysts are also active for the removal of other hetero-atoms such as oxygen and nitrogen from organic molecules in H_2 at elevated temperatures[5]. In particular, the catalytic hydro-deoxygenation (HDO) reaction is becoming industrially more important due to the urgent need for the conversion of oxygen-rich biomass into a renewable hydrocarbon energy source. However, these sulfided catalysts are unstable due to sulfur loss under industrial operating conditions, and without sulfur compensation from an external source, contamination of the products and deactivation of the catalyst is inevitable[6,7]. This has precluded the commercialisation of MoS_2 based catalysts for the hydro-deoxygenation reaction.

To improve catalytic activity and stability, and to mitigate the current need to use of high reaction temperature, a rational bottom-up catalyst design approach following a fundamental understanding of the active site is necessary[8-10]. For example, coordinatively unsaturated edge atoms of nano-crystals are known to offer active sites with promoter atoms for catalysis, whereas coordinatively saturated sites on basal planes of two-dimensional MoS_2 crystals are regarded as catalytically inert[4,11]. However, as the thickness of a MoS_2 crystal is reduced, the proportion of exposed basal plane atoms compared to edge atoms increases dramatically. It is therefore of great significance to also create coordinatively unsaturated sites on the MoS_2 basal plane with promoter atoms, ensuring both basal surfaces and edges are catalytically active.

It is well accepted that layered transition metal dichalcogenides, including MoS_2 and WS_2, can be chemically exfoliated (separated) into single or few layered sheets in solution through intercalation (i.e. using Li), and their band structure can be tailored as a result of changing the s-p_z orbital interactions between their adjacent layers, giving some exceptional optical, electronic and magnetic properties[12-14]. It has recently been shown that chemically exfoliated single MoS_2 molecular layers in fact contain a large concentration of sulfur vacancies on the basal plane due to charge transfer of Li to the layer followed by S^{2-} leaching[15,16]. These sulfur vacancies constitute atomic level interfaces of high surface free energy, onto which small molecules can attach with high affinities, and may thus serve as anchoring sites for metal atoms or clusters. Thiol-terminated ligands have recently been shown to attach to such S-deficient layers strongly by refilling of the sulfur vacancies[17-19].

Here we report the synthesis of a new catalyst consisting of Co dispersed on MoS_2 monolayers, the structure of which is different from those prepared by traditional methods. To prepare this catalyst we first synthesized chemically exfoliated MoS_2 monolayers, followed by mixing these monolayers with thiourea-based Co species via sulfur vacancies. We subsequently show direct experimental evidence that single Co atoms are incorporated into the basal planes. As a result, we demonstrate that the formation of sulfur vacancy sites created by Co on the MoS_2 molecular sheet during hydrogen activation at 300 ^{o}C. This Co-doped monolayer MoS_2 containing many intrinsic sulfur vacancies, displays excellent activity, selectivity and stability for the HDO of 4-methylphenol at 180 ^{o}C with no detectable sulfur loss from the catalyst system.

RESULTS AND DISCUSSION

Structure and Catalytic performance

The preparation of few layer molybdenum disulfide ($^{F}MoS_2$) via solvent intercalation and single layer molybdenum disulfide ($^{S}MoS_2$) via chemical (Li) intercalation of the bulk structure and their Co doping are summarised in the Methods section and in Supplementary Fig. 1. We employed the conversion of 4-methylphenol to toluene in H_2 over these samples in a batch reactor as a typical model for the HDO reaction.

Table 1 shows the comparative catalytic performance of MoS_2 based catalysts for the HDO reaction. Mo based catalysts can provide active surface sites for the HDO of the phenol group via dissociation of the C-O bond. However, as seen

from the literature data, most traditional MoS_2 based catalysts were studied at typical reaction temperatures of 300 ^oC or above (entries 1-3 in Table 1) in order to reach acceptable activities for the HDO of phenolic compounds[6,7,20-22]. A recent study using a slightly lower temperature of 275 ^oC for this reaction (entries 4 and 5) was also noted[23,24]. According to these results, pure MoS_2 gave 91.2% conversion of 4-methylphenol in a 3-h batch reaction, but further decreases in operation temperature proved to be inefficient[23]. The addition of Co atoms was clearly able to promote the reaction, driving it to completion at the same time whilst also achieving greater toluene selectivity. However, these traditionally prepared Co-MoS_2 based catalysts were still inactive at temperatures lower than 275-300 ^oC, presumably as they contained only few catalytically active edge sites in their bulk form[24]. Notice that noble metal containing catalysts are well known to hydrogenate oxygenated organic molecules at much lower temperatures; a fully hydrogenated product, cyclohexane over Pd/ZSM-5 was obtained instead[25] (entry 6).

As seen from entry 9 of Table 1, by merely reducing only the layer thickness of bulk MoS_2 via solvent intercalation[26], our studied $^FMoS_2$ shows 3.8 times higher activity than bulk MoS_2 (entry 7). Electron paramagnetic resonance (EPR) can be used to measure unpaired electrons on coordinatively unsaturated defective sites and can also reflect basal sulfur vacancies present in these layers, because molecular O_2 (from the air) adsorbs at the vacancy and takes up an unpaired electron (peak at g=2.005) from the semi-conductive MoS_2[13]. The EPR characterisation (Supplementary Fig. 1) indicates that a large quantity of defective sites (1.42×10^{17} g^{-1}) are present, presumably on the predominant edges and crystallite interfaces of bulk MoS_2, while the number of exposed sulfur vacancies measured by EPR also increases to 5.44×10^{17} g^{-1} for $^FMoS_2$ (3.8 times). Notice that the measured BET (Brunauer–Emmett–Teller) surface area also increases by about 3.0 times from 8.4 m^2 g^{-1} (bulk MoS_2) to 25.0 m^2 g^{-1} ($^FMoS_2$). Thus, the physical exfoliation of staggered layers from bulk via solvent molecule intercalation increases the surface area of the material by reducing the average layer thickness on a per gram basis. However, the intrinsic defective site concentration predominantly on the sheet edges is not much altered, within experimental error. Thus, most of the freshly exposed basal sites appear to remain fully saturated with sulfur atoms after the solvent exfoliation. Interestingly, single layer $^SMoS_2$ prepared via Li intercalation[27] (entry 10) gives the best activity (98.7%), with its activity 11.7 times higher than the bulk under comparable testing conditions. The increase in sulfur vacancies reflected by EPR is at least 5.4 times (to 7.57×10^{17} g^{-1}), which is significantly higher than expected from the enhancement in surface area (BET surface area of $^SMoS_2$ is 30.5 m^2 g^{-1}, 3.6 times that of the bulk MoS_2). This demonstrates that Li treatment not only increases the relative area of exposed MoS_2 basal surfaces but also promotes the number of sulfur vacancy sites in basal planes.

We expected that the larger number of exposed sulfur vacancies could allow further uptake of Co atoms to enhance catalytic performance. $Co(thiourea)_4^{2+}$ was thus synthesized in-situ with Co acetate in thiourea[28] and used as a source for Co for the reaction with $^SMoS_2$ in hydrothermal conditions, yielding Co-$^SMoS_2$, with a Co loading of 1.8% weight percent (wt%). For comparison, same quantity of Co was also deposited on bulk MoS_2 and $^FMoS_2$, respectively.

All Co-doped catalysts exhibited virtually 100% conversion of 4-methylphenol in the batch reaction at 300 ^oC when using a catalyst concentration of 2 mg mL^{-1} (entry 11, Table 1). In order to follow the rate constant, the concentration of Co-$^SMoS_2$ catalyst was reduced to 0.2 mg mL^{-1} at 300 ^oC. It is evident from entry 11 that the Co immobilization on MoS_2 monolayers as Co-$^SMoS_2$ (396.4 mL s^{-1} mol_{Mo}^{-1}) results in a much higher rate (34 times) compared to non-promoted $^SMoS_2$ (11.7 mL s^{-1} mol_{Mo}^{-1}) despite a small amount of Co doping (also see Figure 1a). This result implies that the immobilized Co on the basal sites of $^SMoS_2$ facilitate the formation of more catalytic sites at a close proximity for cascade catalysis at higher temperature. In terms of activity expressed per mole of Co, the catalyst also displays a superior activity of 7772.5 mL s^{-1} mol_{Co}^{-1} (entry 11), which is 89 times more active than that of the typical

reported $CoMoS_x/Al_2O_3$ catalyst of 87.3 mL s^{-1} mol_{Co}^{-1} (entry 3) under comparable conditions. As far as we are aware, this new catalyst prepared via intercalation shows the highest rate for toluene production among all those catalysts reported in the literature for this reaction.

Upon reducing the operating temperature to 180 ^oC, the Co-$^SMoS_2$ catalyst (entry 13) continues to perform well and achieves high toluene selectivity. Thus, cleavage of [O] from oxygenated compounds in H_2 over this Co doped $^SMoS_2$ catalyst can be achieved even at such a mild temperature. In comparison, Co doped bulk MoS_2 shows a complete substrate conversion at 300 ^oC (entry 8) but is totally inert at 180 ^oC. Co-$^FMoS_2$ shows lower activity at 180 ^oC (entry 12), suggesting that the same quantity of Co does have a greater promotional effect on activity for thinner MoS_2 sheets than bulk. In particular, the best activity is obtained at this temperature when Co is deposited on single layer MoS_2 due to having the highest number of basal sites. This suggests that the atomically dispersed catalyst gives excellent utilization of Mo and Co atoms that are in direct atomic contact, better than that of supported or bulk catalysts prepared by conventional means.

Figure 1b shows the stability test of Co-$^SMoS_2$ at 180 ^oC, 3 MPa of H_2 and 8 h for each batch cycle. The results suggest that there is no obvious deactivation observed after 7 cycles with the addition of a fresh substrate after each cycle for a total reaction time of 56 h. During each cycle the toluene selectivity was maintained at a constant value of 98.5%. In addition, there was no sign of sulfur containing compound in the solution beyond the detection limit of 2 ppm by inductive coupling plasma (ICP) analysis, nor was any pungent smell of H_2S detected. To confirm the chemical stability of the MoS_2, X-ray photoelectron spectroscopy (XPS) was employed, with XPS spectra showing the Mo 3d and S 2p profiles before and after 7 cycles at 180 ^oC (Supplementary Fig. 2). The relative peak ratios and peak positions of Mo 3d and S 2p correspond to the 2H-MoS_2 structure, which remained unchanged after the reaction. In contrast, typical sulfided Mo based catalysts suffer from deactivation caused by sulfur loss with oxidative change of Mo (Mo^{4+} to Mo^{6+}) at elevated temperature[6,7], which our low temperature regime prevents. Moreover, high operating temperatures facilitate coke formation, which is another contributing factor for deactivation in conventional sulfided Mo based catalysts[7]. In sharp contrast, our new Co promoted $^SMoS_2$ materials exhibit exceptional catalytic performance since they are active, selective and stable under low temperature with no apparent loss in sulfur from the catalyst.

Characterisation of MoS_2 monolayer sheets featuring isolated Co atoms (Co-$^SMoS_2$)

The freshly prepared $^SMoS_2$ was characterized by transmission electron microscopy (TEM, Supplementary Fig. 3) and atomic force microscopy (AFM, Supplementary Fig. 4) which indicated that the material contains 56% of its flakes composed of a monolayer, 28% two layers, 13% three layers, and so on[27], with a mixture of turbostratic and well stacked layers[29] (Supplementary Fig. 5). After the Co immobilization on to the dispersed MoS_2 flakes under hydrothermal conditions, some aggregation of the modified sheets was apparent (Supplementary Fig. 3). However, many of the thin-layers of Co-$^SMoS_2$ revealed by high resolution TEM and scanning-mode TEM (STEM) images were monolayer MoS_2 sheets with 2H trigonal prismatic symmetry (Supplementary Figs. 6-8). This was confirmed by our XPS data (Supplementary Fig. 2), in which the 2H phase was exclusively observed[15]. From TEM images (Supplementary Fig. 3), there was no evidence of aggregation of the Co atoms into larger Co-containing nanoparticles on the MoS_2 sheets. This is supported by X-ray diffraction (XRD), which indicated there were no Co containing

crystalline phases present, even though the content of Co in the Co-$^{S}MoS_2$ is 1.8 wt% before and after catalysis (measured by ICP).

The Co chemical environment was then probed by Extended X-ray Absorption Fine Structure (EXAFS), which confirms that the Co does not form into clusters or particles. Figure 2a shows the results of Fourier transforms of Co K-edge EXAFS spectra of Co-$^{S}MoS_2$ in comparison with Co foil and Co(thiourea)$_4$ acetate. The EXAFS parameters are fitted with acceptable Debye-Waller factors (Supplementary Figs. 9 and 10 and Supplementary Table 1). EXAFS shows there is no first-shell Co-Co contribution for the Co-$^{S}MoS_2$ sample, suggesting that the major Co species is not in the form of metallic Co nanoparticles or clusters. Instead, Co-$^{S}MoS_2$ shows a first-shell Co-S contribution with coordination number of about 4 at 2.21 Å, which is slightly shorter than Co-S in molecular Co(thiourea)$_4$ species (2.24 Å). The shortening of average Co-S bond implies a restricted freedom for the Co-S bond upon hydrothermal treatment, which strongly indicates the immobilization of the tetrahedral Co(thiourea)$_4$ complex through at least one of its sulfur ligand atoms to the surface vacant site(s). Interestingly, a new peak at 2.59 Å is found. This is in good agreement with our converged density function theory (DFT) structure for Co atom situated on a Mo atop site of a 2H MoS_2 monolayer via covalent attachment of the sulfur atoms of the thiourea ligand to the sulfur vacant sites, yielding bond lengths for Co-S of 2.13 Å and Co-Mo of 2.57 Å (see DFT model in Figure 4a and Supplementary Fig. 11).

Annular dark field (ADF) imaging by 60 kV STEM combined with electron energy loss spectroscopy (EELS) was used to examine the Co-$^{S}MoS_2$ structure at atomic resolution and to identify the chemical makeup of individual atomic sites[30,31]. ADF-STEM imaging of Co-$^{S}MoS_2$ monolayers revealed sites scattered across the basal plane that were of higher contrast than the surrounding Mo and S_2 sites (Figure 2b, arrows). The Z-contrast nature of ADF imaging implies that this is due to heavier constituent atom(s) in the scanned atomic column. Following from the EXAFS results above indicating the presence of Co situated on Mo atop sites, we simulated the expected ADF image for this Co configuration (Figure 2c) using a DFT-optimised structure (Figure 2d). The simulated image shows good agreement with the experimental image in Figure 2b, as supported by intensity profile analysis (Supplementary Fig. 12).

To further confirm the presence of Co atom in these bright contrast spots simultaneous ADF and EELS acquisitions were performed. A line-scan for both ADF intensity and EELS was taken across a bright contrast spot, indicated in Figure 2e, yielding an ADF intensity profile (Figure 2g). Moreover, Figure 2h depicts EELS extracted from three different positions, indicated by coloured markers in Figure 2f and Figure 2g. These spectra demonstrate the presence of a Co atom in the atomic column (green profile), with the signature $L_{3,2}$ edge occurring at the expected energy levels. Such features are not present in the EELS of the positions above (red profile) and below (blue) the atomic site. Evidence for Co on the Mo atop site was also found by TEM at 80 kV (Supplementary Figs. 6-8) and further HAADF-STEM (Supplementary Fig. 16). In addition to Co being distributed across the basal plane, Co atoms were also detected along the edges of the Co-$^{S}MoS_2$ layers by the simultaneous ADF and EELS mapping (Supplementary Fig. 13).

Interestingly, ADF-STEM imaging of the basal plane of the Co-$^{S}MoS_2$ after catalysis (56 h) provided clear evidence for Co-doping at sites beyond the Mo atop site and the edge site. Figure 3a presents a wide field of view of the Co-$^{S}MoS_2$ basal plane. The characteristic hexagonal pattern of alternating intensity spots (associated with 2H MoS_2 monolayer) is accompanied with regions of blurred contrast corresponding to residue attached to the surface. This residue mostly consists of surface amorphous carbon, which is often observed in samples after catalytic reactions. Intensity profile

analysis of the ADF image taken from the indicated lines (Figure 3b) demonstrates that, in addition to the Co on the Mo site on basal plane, there is evidence for Co being incorporated in place of sulfur, as can be seen in plots 3 and 4. The expected intensities are in agreement with image simulations calculated from DFT geometry optimisations (shown in Figures 3c-e) and are supported by an ADF-EELS simultaneous acquisition line-scan across a Co substitution for S, with the expected $L_{3,2}$ line edge at the Co substitution site (Supplementary Fig. 14). We also observed instances of Co occupying the hollow position in the centre of the MoS_2 hexagon (Figures 3f-h and Supplementary Fig. 15). The three observed configurations for Co incorporating into the MoS_2 basal plane: Co on Mo atop site, Co substituted for S, and Co in the hollow site are confirmed as energetically favourable geometries by DFT (Supplementary Information).

Density functional theory (DFT) calculations

The availability of a large number of additional sites to accommodate Co atoms on basal planes of $^{S}MoS_2$ via sulfur vacancies created from corresponding bulk structure may account for its more efficient catalysis at low temperature. Periodic DFT calculations were thus performed to assess the adsorption energies of Co atom by these sites. First, we found that the chemisorption of Co is exothermic on three site types on the basal plane of 2H $^{S}MoS_2$, namely the Mo atop site, the S atop site, and the hollow site (see Figures 4a-c and DFT calculations in the Supplementary Information), supporting our experimental observations. When Co is highly coordinated on the Mo atop site (Figure 4a), the binding of Co is the most favoured (-2.91 eV) compared to slightly weaker adsorption in the hollow site (-2.63 eV) and much weaker adsorption on the low coordinated S atop site (-1.40 eV). On the Mo atop site, Co is coordinated with three surface sulfur atoms, presumably some of the thiourea ligand(s) of the Co complex refilled the sulfur vacancies on this monolayer. We calculated a short Co-Mo distance, and as discussed, the theoretical Co-S (2.13 Å) and Co-Mo (2.57 Å) distances derived from this refilled Co-Mo atop model fit well with our microscopic and EXAFS data.

We also found that for the single layer 2H-MoS_2 molecular sheet, our calculated energy for sulfur vacancy (V_S) formation is 3.74 eV more favourable than the formation of Mo vacancy (V_{Mo}). Thus, V_S is significantly easier to generate than V_{Mo} from this basal molecular sheet (see Supplementary Information). It is interesting to find that Co adsorbed on a Mo atop site is in fact not stable if a V_S from a neighbouring bridge site is created presumably under elevated temperatures during hydrogen activation period: Co readily moves to fill this V_S and exhibits an adsorption energy of -4.06 eV thereon (Figures 4b, 4d see also DFT calculations in Supplementary Information). Thus, it can become more strongly immobilized as a part of integrated basal atoms, accounting for its remarkable stability observed experimentally. Moreover, this integrated Co atom can further promote new S vacancies in proximal sites in an energetically favourable manner during our hydrogen activation (Figure 4e) due to the electronic promotion effect of Co-Mo (presumably with the mixing of d-orbitals of Co with Mo) as discussed in the Supplementary Information (also see Supplementary Figs. 17-20). Indeed, STEM-EELS and image simulation (Figures 2 and 3) confirmed the presence of all calculated Co sites in the post-reaction Co-$^{S}MoS_2$ sample (Co on edge, Co atop to Mo; Co on V_S; Co on hollow site, etc). The low V_S formation energy at the interface of Co-[S]-Mo on the edge site has previously been discussed[3,32].

The availability of coordinatively unsaturated sulfur vacancies and hollow basal sites to accommodate additional Co atoms in this unconventionally prepared single molecular layer MoS_2, akin to the edge site are clearly evident. Indeed, we have showed Co atoms can take residence on both the edge sites and basal sites of Co-$^{S}MoS_2$. Early studies had

pointed to the edges as being the active sites. However, this view has recently been challenged and basal S vacancies have been proposed as possible instigators of chemical reactivity of the MoS_2 basal plane[33-35]. Although our present data reveals that the general increase in basal S vacancies can contribute toward catalytic activity, it may not be conclusive in showing exactly which sites are active and to what degree they contribute to the overall activity and that we cannot exclude the possibility that catalysis is dominated by the edges. However, the much larger number of basal versus edge sites and the fluxional (dynamic) behaviour of Co at elevated temperatures, being able to diffuse between edges and basal planes, means that a sizeable population of Co atoms resides in these planes facilitating the formation of sulfur vacancies. Thus, the dramatic increase in the activity of $^{S}MoS_2$ towards HDO of 4-methylphenol upon Co promotion, must be related to the consequent wider availability of these basal vacant sites, which act as catalytically active centres for this reaction. Finally, we assessed the tendency of sulfur loss of the Co-$^{S}MoS_2$ catalyst (see Supplementary Information). In both the pristine and Co-promoted $^{S}MoS_2$, S-loss is uphill in energy, whereas HDO is exothermic when oxygenated compound is present. This calculation supports the lack of sulfur loss and the stability of the catalyst observed during the HDO of 4-methylphenol.

Conclusions

In summary, a strong covalent attachment of Co atoms to monolayer MoS_2 through defect engineering significantly enhances the number of active Co-S-Mo interfacial sites on the basal plane (Co on atop site to Mo, Co in hollow site and Co substituting S site, etc), as shown by STEM and EELS. In this work, we employed the strategy of creating a large number of basal sulfur vacancies within Co-doped single-layer MoS_2 through high-temperature treatment in H_2 (300 ^{o}C), which provided a sufficient number of Co-S-Mo active sites for the HDO reaction to occur at a low operating temperature (180 ^{o}C). The catalyst described is extremely active, selective and stable for the conversion of 4-methylphenol to toluene in hydrogen at low operation temperature and opens the possibility of using this novel type of catalyst for hydro-deoxygenation for biomass conversion without sulfur loss from the catalyst.

Methods

Preparation of single-layered MoS_2 ($^{S}MoS_2$). In a typical experiment, 0.5 g of bulk MoS_2 crystalline powder was soaked in 4 mL of 1.6 M n-butyllithium/hexane for 48 h under nitrogen atmosphere. After the intercalation of MoS_2 by lithium, the produced Li_xMoS_2 was washed using vacuum filtration with 50 mL of hexane to remove excess butyllithium and organics and then dried under N_2. Then the powder was immersed into 250 mL of water and the resulting suspension was sonicated to assist the completion of the exfoliation process, as any intercalated lithium would react with water to form H_2 gas between the layers. The evolution of H_2 tended to assist the separation of MoS_2 layers. The dispersion was centrifuged at 5000 rpm for 15 min to remove unexfoliated precursor and only the supernatant was collected by pipette. Eventually, the exfoliated MoS_2 layers remained totally suspended in aqueous solution. The pH value of the dispersion became alkaline due to the presence of trace of lithium hydroxide. To collect the $^{S}MoS_2$ powder a proper amount of HCl solution was added dropwise into the above colloid till the pH value reached around 7. The precipitate was then washed and collected by centrifugation several times and the final product was dried under vacuum for 12 h.

Preparation of Co-$^{S}MoS_2$ catalyst. The isolated Co atom promoted $^{S}MoS_2$ (Co-$^{S}MoS_2$) catalyst was prepared using a hydrothermal method. 50.6 mg of cobalt acetate tetrahydrate and 36 mg of thiourea were added into 1 mL of water for overnight to form the complex Co ion ($Co(thiourea)_4^{2+}$)[28]. Subsequently this Co thiourea complex solution was then added into 50 mL of 1 mg mL^{-1} stabilized $^{S}MoS_2$ colloid (30 v/v% isopropanol/water with 50 mg of polyvinylpyrrolidone). A mixed homogeneous solution was then transferred to an autoclave, followed by hydrothermal treatment at 160 ^{o}C for 24 h. In order to anchor Co atoms onto the defects of $^{S}MoS_2$ rather than inducing a fast self-nucleation, we used a very low concentration of the Co complex. During the hydrothermal process, the thiourea- Co complex refilled some of the surface sulfur vacancy sites of $^{S}MoS_2$. Previous works confirm that defective vacancy sites possess high molecular affinity, especially for thiol-based molecules[17-19]. After the reaction, the precipitate was washed three times using deionized water and then dried under vacuum for 12 h and finally pretreated with H_2 at 300^{o}C for 1 h prior to storage.

Preparation of $^{F}MoS_2$. 6 g of bulk MoS_2 powder was dispersed into 400 mL of isopropanol/water, and 4 mL of hydrazine monohydrate[26]. The system was sonicated for 12 h, and was then centrifuged at 2000 rpm for 60 min to remove non-exfoliated sediments. In order to collect the exfoliated $^{F}MoS_2$ powder from suspension, we changed the pH to around 7 by adding HCl solution. The charge balance in the dispersion would be disrupted, which would cause a fast flocculation. The final products were centrifuged, washed with deionized water by three times, and dried in the vacuum container for 12 h.

Hydrodeoxygenation (HDO) reaction of 4-methylphenol (4-MP). The HDO reaction of 4-methylphenol was carried out in a 50 mL sealed autoclave reactor (Parr 4792. pressure vessel) with an inner glass liner. In a typical procedure, 280 mg of 4-methylphenol, 20 mg of catalyst and 280 mg of octane (internal standard) were dispersed in 10 mL decalin and then transferred to the reactor. Then the autoclave was purged by H_2 for several times, then pressurized to 3 MPa and heated to chosen temperature. After reaction, the autoclave was cooled down naturally to room temperature. A small volume of liquid sample was collected and then analyzed by gas chromatography (Agilent 6890N). The products were confirmed against pure samples and mass spectrometry (MS). For all the experimental data, the carbon balance was >95% and experiments were repeated at least three times to ensure the repeatability of the data. The rate of the HDO of 4-methylphenol was calculated assuming a pseudo-first-order reaction as below,

$$ln(1-x) = -kC_{cat}t \quad (1)$$

where k is the pseudo-first-order rate constant (mL s^{-1} mol^{-1}), x is the conversion of 4-methylphenol, C_{cat} is the concentration of catalyst under reaction system and t is the reaction time (s).

Sample characterisations as well as the theoretical methods and computational details, are described in the Supplementary Information.

Data availability statement:

All relevant data are available from the corresponding author (SCET) and detailed supplementary information containing sections of methods descriptions; supplementary Figs. 1-20 with results and discussions; assessment of electronic influence; DFT calculations; anticipated advantages of the new catalyst, background of the desulfurization reaction and references are included with the manuscript.

References and Notes:

1. Prins, R., De Beer, V. H. J. & Somorjai, G. A. Structure and function of the catalyst and the promoter in Co-Mo hydrodesulfurization catalysts. *Catal. Rev.-Sci. Eng.* **31**, 1-41 (1989).
2. Grange, P. Catalytic hydrodesulfurization. *Catal. Rev.-Sci. Eng.* **21**, 135-181 (1980).
3. Byskov, L. S., Nørskov, J. K., Clausen, B. S. & Topsøe, H. DFT calculations of unpromoted and promoted MoS_2-based hydrodesulfurization catalysts. *J. Catal.* **187**, 109-122 (1999).
4. Karunadasa, H. I. *et al.* A molecular MoS_2 edge site mimic for catalytic hydrogen generation. *Science* **335**, 698–702 (2012).
5. Elliott, D. C. Historical developments in hydroprocessing bio-oils. *Energy Fuels* **21**, 1792−1815 (2007).
6. Saidi, M. *et al.* Upgrading of lignin-derived bio-oils by catalytic hydrodeoxygenation. *Energy Environ. Sci.* **7**, 103–129 (2014).
7. Ruddy, D. A. *et al.* Recent advances in heterogeneous catalysts for bio-oil upgrading via "ex situ catalytic fast pyrolysis": catalyst development through the study of model compounds. *Green Chem.* **16**, 454–490 (2014).
8. Qiao, B. *et al.* Single-atom catalysis of CO oxidation using Pt_1/FeO_x. *Nat. Chem.* **3**, 634-641 (2011).
9. Chen, G. *et al.* Interfacial effects in iron-nickel hydroxide–platinum nanoparticles enhance catalytic oxidation. *Science* **344**, 495-499 (2014).
10. Lin, J. *et al.* Remarkable performance of Ir_1/FeO_x single-atom catalyst in water gas shift reaction. *J. Am. Chem. Soc.* **135**, 15314−15317 (2013).
11. Jaramillo, T. F. et al. Identification of active edge sites for electrochemical H_2 evolution from MoS_2 nanocatalysts. Science 317, 100–102 (2007)
12. Chhowalla, M. *et al*. The chemistry of two-dimensional layered transition metal dichalcogenide nanosheets. *Nat. Chem.* **5**, 263-275 (2013).
13. Cai, L. *et al.* Vacancy-induced ferromagnetism of MoS_2 nanosheets. *J. Am. Chem. Soc.*, **137**, 2622–2627 (2015).
14. Mak, K. F., Lee, C., Hone, J., Shan, J. & Heinz, T. F. Atomically thin MoS_2: A new direct-gap semiconductor. *Phys. Rev. Lett.* **105**, 136805 (2010).
15. Eda, G. *et al.* Photoluminescence from chemically exfoliated MoS_2. *Nano Lett.* **11**, 5111−5116 (2011).
16. Eda, G. *et al.* Coherent atomic and electronic heterostructures of single-layer MoS_2. ACS Nano **6**, 7311−7317 (2012).
17. Makarova, M., Okawa, Y. & Aono, M. Selective adsorption of thiol molecules at sulfur vacancies on MoS_2 (0001), followed by vacancy repair via S-C dissociation. *J. Phys. Chem. C* **116**, 22411−22416 (2012).
18. Yu, Z. *et al.* Towards intrinsic charge transport in monolayer molybdenum disulfide by defect and interface engineering. *Nat. Commun.* **5**, 5290 (2014).
19. Chou, S. S. *et al.* Ligand conjugation of chemically exfoliated MoS_2. *J. Am. Chem. Soc.* **135**, 4584−4587 (2013).
20. Wang, C., Wu, Z., Tang, C., Li, L. & Wang, D. The effect of nickel content on the hydrodeoxygenation of 4-methylphenol over unsupported NiMoW sulfide catalysts. *Catal. Commun.* **32**, 76–80 (2013).
21. Whiffen, V. M. L., Smith, K. J. & Straus, S. K. The influence of citric acid on the synthesis and activity of high surface area MoP for the hydrodeoxygenation of 4-methylphenol. *Appl. Catal. A* **419– 420**, 111–125 (2012).
22. Gevert, B. S., Otterstedt, J-E. & Massoth, F. E. Kinetics of the HDO of methyl-substituted phenols. *Appl. Catal.* **31**, 119–131 (1987).
23. Wang, W. *et al.* Influence of surfactants on the synthesis of MoS_2 catalysts and their activities in the

hydrodeoxygenation of 4-methylphenol. *Ind. Eng. Chem. Res.* **53**, 10301−10309 (2014).
24. Wang, W. *et al.* Synthesis of highly active Co-Mo-S unsupported catalysts by a one-step hydrothermal method for p-cresol hydrodeoxygenation. *Ind. Eng. Chem. Res.* **53**, 19001−19009 (2014).
25. Zhao, C. & Lercher, J. A. Selective hydrodeoxygenation of lignin-derived phenolic monomers and dimers to cycloalkanes on Pd/C and HZSM-5 catalysts. *ChemCatChem* **4**, 64–68 (2012).
26. Liu, G. *et al.* Hydrazine-Assisted Liquid Exfoliation of MoS_2 for Catalytic Hydrodeoxygenation of 4-Methylphenol, *Chem. Eur. J.*, **22**, 2910-2914 (2016).
27. Jia, T. *et al.* The remarkable activity and stability of a dye-sensitized single molecular layer MoS_2 ensemble for photocatalytic hydrogen production. *Chem. Commun.* **51**, 13496-13499 (2015).
28. Spofford, W. A. & Amma, E. L. Crystal and molecular structure of tetrakisthiourea cobalt (II) nitrate monohydrate, C4H16CoN8S42+,2NO3-,H2O. *J. Cryst. Mol. Struct*. **6**, 235-258 (1976).
29. Warner, J. H., Rümmeli, M. H., Gemming, T., Büchner, B. & Briggs, G. A. D. Direct imaging of rotational stacking faults in few layer graphene. *Nano Lett*. **9**, 102–106 (2009).
30. Krivanek, O.L. *et al.* Atom-by-atom structural and chemical analysis by annular dark-field electron microscopy. *Nature* **464**, 571-574 (2010).
31. Lin, Y. C. et al. Properties of individual dopant atoms in single-layer MoS_2: Atomic structure, migration, and enhanced reactivity. *Adv. Mater*. **26**, 2857-2861 (2014).
32. Zhu, Y. et al. Visualizing the stoichiometry of industrial-style Co-Mo-S catalysts with single-atom sensitivity. *Angew Chem. Int. Ed.* **53**, 10723-10727 (2014).
33. Le, D., Rawal, T. B. & Rahman, T. S. Single-layer MoS_2 with sulfur vacancies: structure and catalytic application. *J. Phys. Chem. C* **118**, 5346-5351 (2014).
34. Komsa, H. P. & Krasheninnikov, A. V. Native defects in bulk and monolayer MoS_2 from first principles. *Phys. Rev. B* **91**, 125304 (2015).
35. Farias, M. H., Gellman, A. J., Somorjai, G. A., Chianelli, R. R. & Liang, K. S. The CO coadsorption and reactions of sulfur, hydrogen and oxygen on clean and sulfided Mo (100) and on MoS_2(0001) crystal faces. *Surf. Sci.* **140**, 181-196 (1984).

Acknowledgments:
The financial support of this project from the EPSRC research council of UK is acknowledged. The authors wish to thank the National Synchrotron Radiation Center, Hsinchu, Taiwan (Yun-Liang Soo and Tai-Sing Wu) for accessing EXAFS facilities. A.W.R acknowledges a financial support from KIER (B6-2452). YCL and KS thank for the support from the JST Research Acceleration Programme. The authors also acknowledge the use of the UCL Legion High Performance Computing Facilities Legion@UCL and Grace@UCL, and associated support services, in the completion of the theoretical part of this work.

Authors' contributions:
GL performed synthesis, catalyst testing and material characterizations; MMJL carried out EXAFS analysis; WCHK carried out HAADF-STEM analysis; AWR and JHW performed AC-TEM analysis; AWR, YCL and KS for STEM-EELS analysis; MTD, MHM and MS for DFT calculations; GL, AWR and SCET wrote the main manuscript text; all authors discussed and reviewed this paper. SCET planned, supervised and leaded this whole project as the corresponding author.

Additional Information:
Competing financial interests: The authors declare no competing financial interests in this work.

Figure Captions:

Figure 1. Superior activity and stability of Co-$^{S}MoS_2$. a, A kinetic study of 4-methylphenol to toluene showing activity order of Co-$^{S}MoS_2$ > $^{S}MoS_2$ > $^{F}MoS_2$ > bulk MoS_2. Co-$^{S}MoS_2$ yields a rate 34 times higher than that of bare $^{S}MoS_2$ at 3 MPa and 300 ^{o}C. Note: the concentration of the Co-$^{S}MoS_2$ catalyst in the reaction was set at 0.2 mg mL^{-1} while the others were kept at 2 mg mL^{-1}; the errors of each conversion (after t hour) are estimated to be within ±1%. **b,** Stability test of Co-$^{S}MoS_2$ for HDO of 4-methylphenol. Reaction conditions: 3 MPa at 180 ^{o}C.

Figure 2. Chemical characterisation and identification of the Co atom in fresh Co-$^{S}MoS_2$ by EXAFS and ADF-STEM and EELS. a, Fourier transforms of k^3-weighted Co K-edge of X-ray absorption fine structure spectroscopy (EXAFS) spectra of Co-$^{S}MoS_2$, Co(thiourea)$_4$ and Co foil. **b,** ADF-STEM image of Co-$^{S}MoS_2$, showing two bright contrast sites in the MoS_2 monolayer (arrows). **c,** An ADF image simulation, and **d,** corresponding atomic model, from geometry optimised DFT of a single Co on Mo atop site, showing good agreement with (b). **e,** ADF-STEM image of Co-$^{S}MoS_2$. Scale bar 0.5 nm. **f,** a magnified view of a Co atom on Mo atop site (boxed area of **e**). **g, h,** Simultaneous acquisition (g) ADF and (h) EELS acquired along the line in (**f**), with EELS extracted from above (red), on (green), and below (blue) the Co atom on Mo atop site. The $L_{3,2}$ edge for Co are indicated, confirming the scanned atomic column contains a Co atom.

Figure 3. Detailed atomic resolution ADF-STEM characterisation of the basal plane of used Co-$^{S}MoS_2$. a, ADF image of the basal plane of Co-$^{S}MoS_2$ (post-catalysis). Scale bar 0.5 nm. **b,** ADF intensity line profiles taken along the appropriately numbered lines indicated in (a) (scatter plots). Solid line plots are from corresponding image simulations (see Supporting Information). Red arrows in plots 3 and 4 indicate sample drift during image acquisition. **c,** ADF image of a Co-substituted S site. **d,** Image simulation, and **e,** atomic model, from geometry optimised DFT of a Co-substituted S site. **f,** ADF image, **g,** image simulation from DFT geometry optimisation, and h, atomic model from DFT, showing Co in the hollow site.

Figure 4. DFT optimised geometries of the three Co binding configurations and the energetics of how the Co-S-Mo interface promotes the formation of more sulfur vacancy sites. a-c, Top, side, and perspective views of the DFT calculated geometries for Co on the **a**, Mo atop site, **b**, S substitution, and **c**, hollow site of monolayer MoS_2. **d,** Co-Mo at the interface of Co-[S]-Mo at elevated temperature can create a sulfur vacancy at the bridge site, which can then be readily filled by the Co atom. This process is energetically favourable (exothermic). **e,** Co-substituted S (black sphere) can promote new sulfur vacancies in proximity sites, as evidenced by the lower sulfur vacancy formation energies compared to the reference case of infinitely separated Co and S-vacancy, due to the electronic influence of Co-Mo (see Supplementary Information).

Table 1 Comparison of HDO reactivity in the conversion of 4-methylphenol to toluene for MoS_2 with and without Co, along with other HDO catalysts from the literature (T is temperature; P is pressure; t is time; *k* is pseudo-first-order reaction rate).

Entry	Catalyst	Conditions			Catalytic performance				Ref.
		T (^{o}C)	P (MPa)	t (h)	Conv. (%)	Toluene select. (%)[a]	*k* (mL s^{-1} mol$_{Mo}^{-1}$)[b]	*k* (mL s^{-1} mol$_{Co}^{-1}$)[b]	
1	$NiMoWS_x$	300	3.0	5	97.8	87.2	17.0	N/A	*20*
2	MoP	350	4.4	5	71.0	51.0	1.3	N/A	*21*
3	$CoMoS_x/Al_2O_3$	300	5.0	N/A	N/A	N/A	47.0	87.4	*22*
4	MoS_2	275	4.0	3	91.2	73.8	N/A	N/A	*23*
5	$CoMoS_x$	275	4.0	4	100	92.2	N/A	N/A	*24*
6	Pd/ZSM-5	200	5.0	2	100	100[c]	N/A	N/A	*25*
7	Bulk-MoS_2	300	3.0	6	25.8	94.0	1.0	N/A	this work

8	Co-bulk-MoS_2[e]	300	3.0	6	100	90.5	N.D.	N/A	This work
9	$^{F}MoS_2$	300	3.0	6	69.6	87.2	3.8	N/A	this work
10	$^{S}MoS_2$	300	3.0	5	98.7	83.1	11.7	N/A	this work
11	Co-$^{S}MoS_2$ [d]	300	3.0	1	83.6	99.2	396.4	7772.5	this work
12	Co-$^{S}MoS_2$	180	3.0	8	97.6	98.4	5.6	109.8	this work
13	Co-$^{F}MoS_2$	180[e]	3.0	2	21.0	98.0	2.7	52.9	this work

[a] methylcyclohexene and methylcyclohexane as main side products; [b] initial activity is expressed as the amount (mL) of 4-methylphenol per mole of Mo or Co with no depletion of substrates at low conv. (see Fig. 2a). Higher activity reflects larger number of surface sites for catalysis; [c] 100% selectivity to cyclohexane. [d] near 100% yield at 2 mg mL^{-1}; to follow this high rate constant, concentration of this catalyst was reduced to 0.2 mg mL^{-1} at 300 ^{o}C. [e] no activity for Co-bulk MoS_2 at 180 ^{o}C. $^{S}MoS_2$ refers to mono- (single-) layer MoS_2 sheets, and $^{F}MoS_2$ few-layer MoS_2.

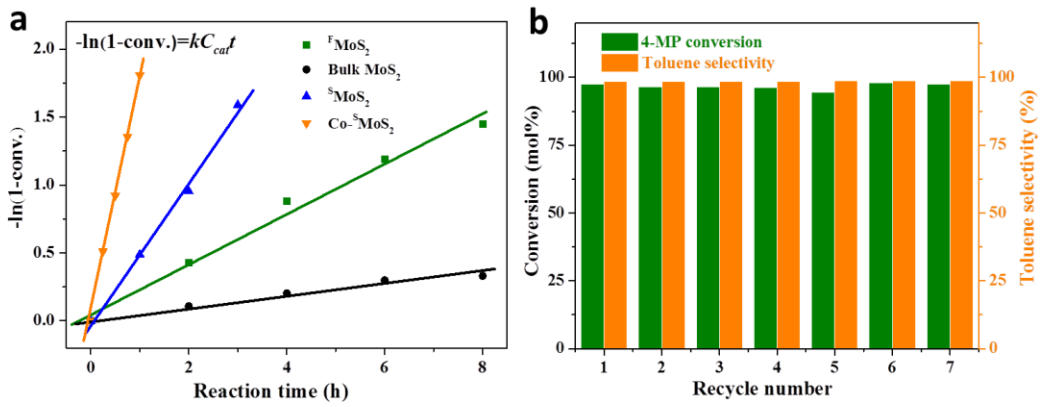

Figure 1.

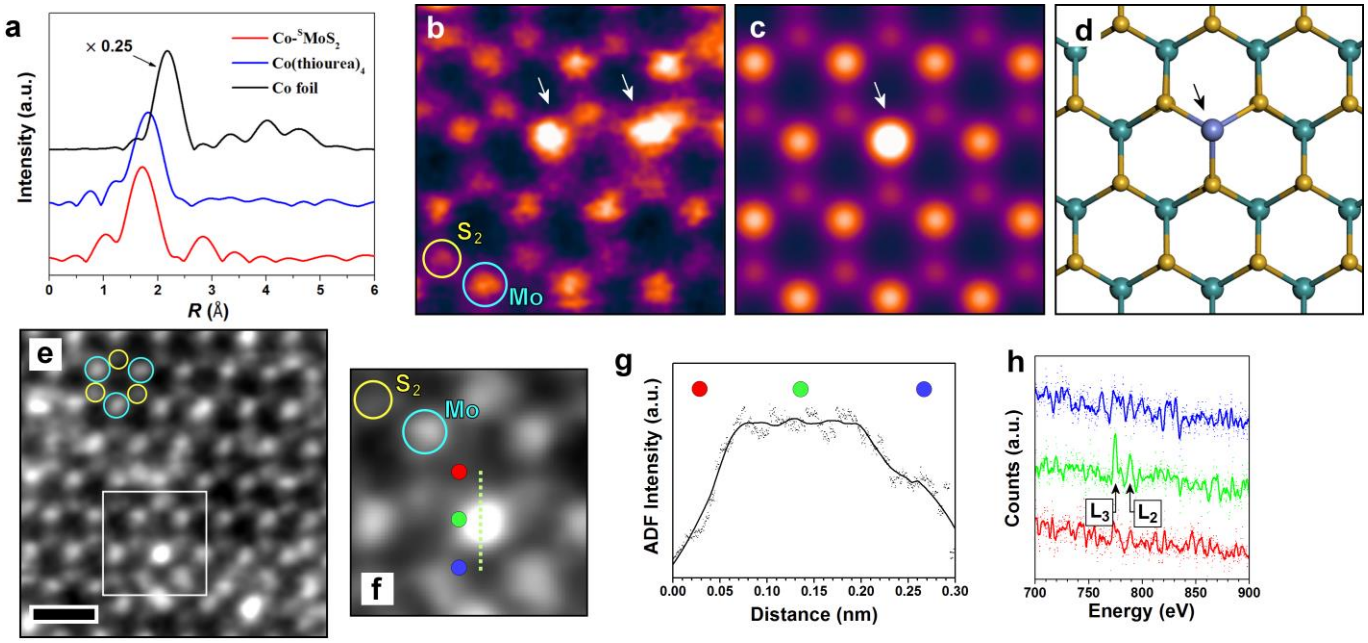

Figure 2.

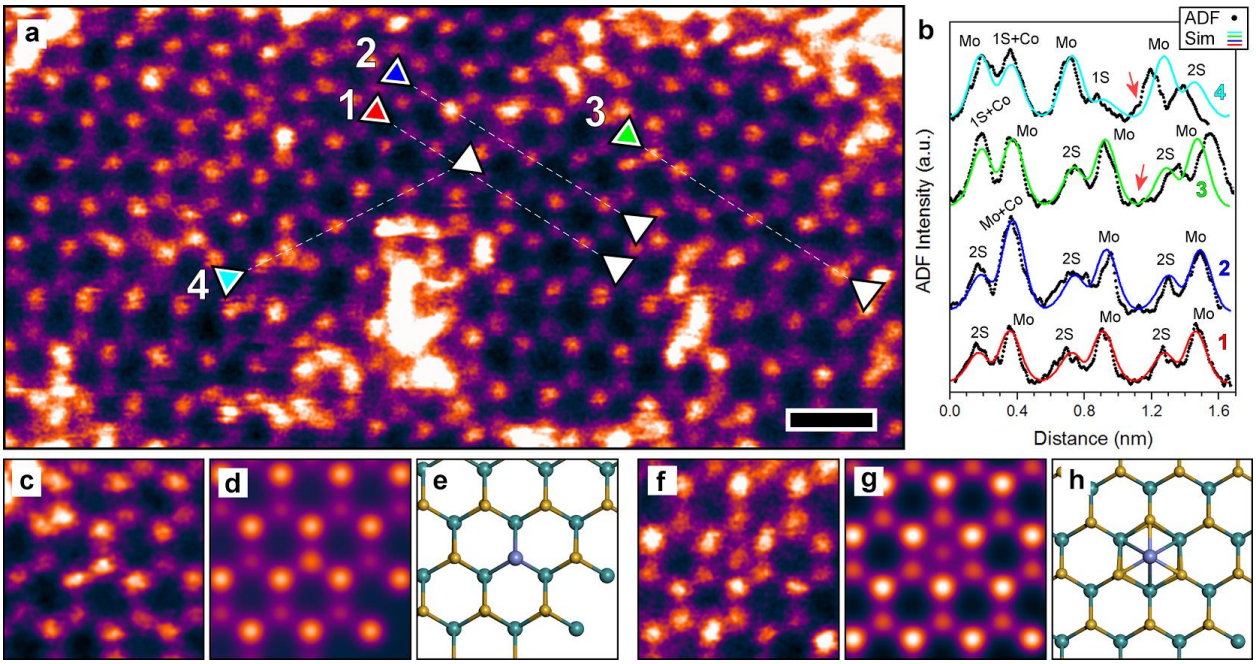

Figure 3.

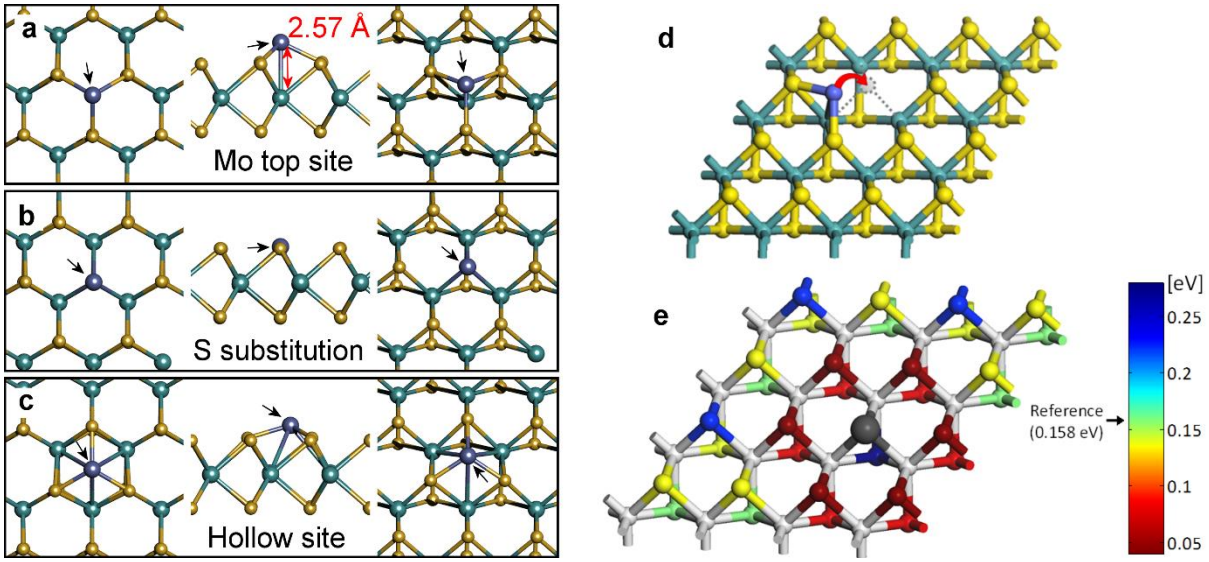

Figure 4.